A simplified numerical model of PCM water energy storage

Kong, Weiqiang; Wang, Gang; Englmair, Gerald; Nielsen, Elsabet Nomonde Noma; Dragsted, Janne; Furbo, Simon; Fan, Jianhua

Published in:
Journal of Energy Storage

Link to article, DOI:
10.1016/j.est.2022.105425

Publication date:
2022

Document Version
Publisher's PDF, also known as Version of record

Journal of Energy Storage 55 (2022) 105425

Contents lists available at ScienceDirect

Journal of Energy Storage

journal homepage: www.elsevier.com/locate/est

Research papers

A simplified numerical model of PCM water energy storage

Weiqiang Kong *, Gang Wang, Gerald Englmair, Elsabet Nomonde Noma Nielsen, Janne Dragsted, Simon Furbo, Jianhua Fan

Department of Civil and Mechanical Engineering, Technical University of Denmark, Brovej 118, 2800 Kgs. Lyngby, Denmark

ARTICLE INFO

Keywords:
Phase change material
Energy storage
Numerical simulation
Implicit method
Supercooling

ABSTRACT

A generic numerical model of PCM water energy storage is developed and validated by experiments. The numerical model consists of a water region and a PCM region. Models of the two regions are derived by the energy differential equations and solved by the implicit method. The solid-liquid PCM behavior is modeled based on its enthalpy-temperature relation, in which the melting/solidification phase is linearized. Special treatment is developed for the time steps with a phase change, which significantly improves the prediction accuracies of PCM temperatures and the melting fractions. An iteration method is applied to the two regions for coupling calculation. The energy balance of the model is examined in each time step. Extended functionalities of the numerical model are further developed, including separate heat loss coefficients, auxiliary heaters, flexible inlet and outlet layout, the mixing effect in the water tank, and three PCM supercooling-activation modes. The experimental verification for a PCM water energy storage was carried out at Technical University of Denmark. The PCM and water layer temperatures are calculated. The simulated and measured outlet temperatures and heat content are compared. The results show that the simulated outlet temperatures are maximum of 4.6 K deviation from the measured, with a relative error of 10.4 %. The relative error of the heat content is within 1 %, and the energy balance errors are within 5 %. The extended application and limitation of the numerical model are discussed, and the possible error sources are analyzed.

1. Introduction

Energy storage plays an important role in renewable energy development and utilization. Compared to other energy storage technologies, thermal energy storage has the advantages of high energy density, large installed capacity, low cost, and long service life [1]. Phase Change Material (PCM) energy storage systems take further advantages of utilizing both the sensible and latent heat in flexible manners, which can further increase system efficiency and reduce the space demand. Currently, PCM energy storage is widely studied and applied in different applications, i.e., solar heating and cooling systems [2–7], solar cookers [8,9], thermal comfort in buildings and vehicles [10–13], thermal protection of food and electronics, and medical applications [14].

Numerical simulation is a powerful tool to estimate the thermal performance of PCM energy storages and systems. Computational Fluid Dynamics (CFD) is suitable for simulating complex shapes or designing new PCM energy storage concepts [15]. However, CFD simulation typically costs a long time in the detailed calculation for the heat transfer and fluid flow, which is not a good option in the system simulation that contains PCM energy storage. The other method is to self-develop numerical models of PCM energy storage - either a specific model for a certain case or a general model for general purposes. There is a lot of literature on developing different kinds of specific numerical models for specific scenarios. For example, Ljungdahl et al. [16] present an active cooling application utilizing a PCM module for the purpose of air conditioning. The apparent heat capacity method is used for modeling the PCM behavior. The hysteresis of the PCM is determined by a generalized logistic function for the melting fraction of the PCM. Separate experiments are needed to determine the parameters in the logistic function for the heating and cooling processes. Filonenko et al. [17] developed an open-source Modelica package [18] for a specific type of PCM ventilation unit. The 0D PCM ventilation unit model is also based on the apparent heat capacity model concept, which converts the nonlinear differential equation of the PCM heat exchanger to the usual state-space form and models it by using the standard thermal RC components from the Modelica Standard Library. The model aims to be mainly used as control and emulator models in the model predictive control applications. Morales-Ruiz et al. [14] present a numerical model of a PCM plate energy storage unit with a particular configuration used in an actual

* Corresponding author.
E-mail address: weiko@dtu.dk (W. Kong).

https://doi.org/10.1016/j.est.2022.105425
Received 10 May 2022; Received in revised form 15 July 2022; Accepted 30 July 2022
Available online 4 August 2022

Nomenclature

A	area, m^2
c	specific heat capacity, J/(kg·K)
E_L	latent heat of fusion, J/kg
Er	error, %
h	heat transfer coefficient, W/(m^2·K)
H	enthalpy, J/kg
k	thermal conductivity, W/(m·K)
Q	power, W
m	mass, kg
$\dot{m}$	mass flow rate, kg/s
t	time, s
T	temperature, °C
u	Inlet flow velocity, m/s
V	volume, m^3
x	Layer/node distance, m

Greek symbols

Δ	difference, –
ρ	density, kg/m^3
Γ	overall heat transfer coefficient, W/(m^2·K)

Subscripts

a	ambient
aux	auxiliary
c	cross area
exp	experiment
m	melting/mean
i	the ith layer
p	PCM
s	side area
sim	simulation
pw	PCM-water heat exchange area
t	tank
hl	heat loss
w	water

household application. The numerical model consists of the fluid flow, the plate and the PCM. The thermal behavior of the PCM is solved by means of the conservative mass, momentum and energy (entropy) equations. Tao et al. [19,20] developed a numerical model for PCM energy storage with a shell and tube configuration. The energy equation for PCM is also based on the entropy method.

However, there is far less research on developing generic models for PCM energy storage. IEA SHC Task 32 subtask C [21,22] organized three teams to develop generic numerical models for PCM energy storage that can be used in the simulation environment TRNSYS [23]. It aimed to develop optimized systems with various PCM energy storage, hydraulics, and control configurations. The published models are summarized in the following.

Type 860 [2,24,25] is a TRNSYS component simulating heat transfer in PCM plugged in water tank storage. It was developed based on an existing TRNSYS water tank (type 60). The PCM modules can be defined as different shapes such as cylinders, plates, or spheres bed. The heat conduction and convection of PCM and water were taken into account as well as the PCM hysteresis and supercooling degree.

The PCM part uses the enthalpy method, in which the temperature – enthalpy curve is divided into five linear lines. Calculation of PCM temperatures is a sub-loop or sub time step under the main loop of water tank calculation. The model simulates a 2D PCM shape and calculates a detailed heat transfer inside the PCM and the interaction between PCM and water. However, the model needs hundreds of parameters provided by users, and the calculation time needs to be concerned by increasing nodes. Further, an explicit solving method was chosen, leading to a simple calculation process but resulting in a conditionally steady condition and possibly divergence problem. Therefore, proper time step and calculation efficiency need to be pre-considered.

Type 840 [22,26] models detailed water tanks with integrated PCM modules of different geometries or tanks filled with PCM slurry. The multi-node storage model calculates one dynamic enthalpy equation. PCM is modeled as one built-in term in the equation calculating the heat transfer between the storage fluid and the PCM and the heat transfer inside the PCM by conduction as well as the phase change processes. The other terms model the inlet-outlet flow, heat exchanger, auxiliary heater, conduction effect, and heat losses. The PCM is subdivided into a 1D (sphere) or 2D (cylinder, plate) nodal network. Further, the PCM hysteresis and supercooling degree phenomenon are also modeled. However, the model uses the explicit method for solving the governing equations, and the thermal properties of the PCM are read from ASCII data files provided by users.

Type 841 [22] models a bulk PCM storage tank with an immersed heat exchanger. The heat exchanger is built as a fin-tube type. The heat transfer fluid flows at high speed in the tube, and the PCM is outside the tube. The heat exchange capacity rate between PCM and fluid is increased by the fins. Unlike type 840, the volume of a storage node does not include the volume of the heat transfer fluid in the tube, and the enthalpy temperature relation of PCM uses three linear functions for the solid, liquid, and phase change region. However, this model also used the explicit method, which is not unconditionally stable. The time step must be maintained below a certain limit.

Type 185 [22] is another simulation program that models the bulk PCM storage tank with immersed heat exchangers. It features by simulating the PCM stable supercooling phenomenon as well as flexible control strategies. The model does not consider the heat conduction between PCM nodes. A particular method was built into the model to enhance the convergence, and some minor theoretical errors exist.

Belmonte et al. [27] proposed a simplified method for modeling the performance of a thermal energy storage (TES) system that contains PCM. The developed approach is similar in concept to the bypass factor method. The method provides reasonably accurate results while requiring only the most relevant input parameters (a total of 10) commonly available during the early stages of TES system design. The method is particularly suitable for application during preliminary stages and is generally applicable to any TES system with a PCM, thereby simplifying the performance characterization and implementation of such TES systems in energy analysis tools such as TRNSYS.

This paper aims to develop a generic numerical model for PCM water energy storages that can be used in system simulation with a good balance of accurate results and fast calculation. The configuration of the PCM water energy storage can be flexible. In Section 2, the water and PCM regions of the energy storage are modeled separately by 1D energy differential equations. The two models are discrete by the finite difference technique using the implicit method. The solid-liquid PCM behavior is described by its enthalpy-temperature relation, in which the melting/solidification phase is linearized. The converged temperatures of water and PCM are obtained by solving the two models in an iteration way. In Section 3, extended functionality of the energy storage model is further developed, including the separate heat loss coefficients, auxiliary heaters, flexible inlet and outlet layout, the mixing effect in the water tank, and three PCM supercooling - activation modes. Section 4 describes the experimental verification carried out at Technical

University of Denmark. The PCM water energy storage, the test facility, and the test method are introduced. The water and PCM temperatures at each layer of the energy storage were calculated. The simulated and measured outlet temperature and the charged and discharged heat were compared. In Section 5, the application and limitation of the numerical model are discussed, and the possible error sources are analyzed.

2. Mathematical model

The mathematical model consists of the water region model, the PCM region model, and the coupling iteration method. The water and PCM region models can also be used separately for simulating a single water tank or a single PCM tank. The schematic diagram of energy storage is illustrated in Fig. 1. The energy storage tank is assumed as a cylinder tank. The water and the PCM in the tank are at the same height and divided into n layers of equal size. The first layer is on the top, and the last layer is at the bottom. The water tank is at the outer of the energy storage, and PCM is located inside of the tank and surrounded by water. The flow inlet and outlet are at the first and the last layer. The tank wall materials are not considered in the model. The radial heat conduction in the water and the PCM region is neglected. Therefore, the water in one layer is assumed to have the same temperature, so as the PCM.

It is assumed a uniform flow distribution in the flow direction inside the energy storage. Therefore, only energy equations are considered. The energy models are calculated by the finite difference method in the implicit formulation. The modeling of the phase change from solid to liquid is based on the enthalpy method. The heat convection in the liquid PCM region is not considered in the model. The modeling and the calculation method are specified in the following sub-sections.

2.1. The water region

Take the cylinder PCM water tank shown in Fig. 1 as an example to illustrate the mathematical model and the calculation method.

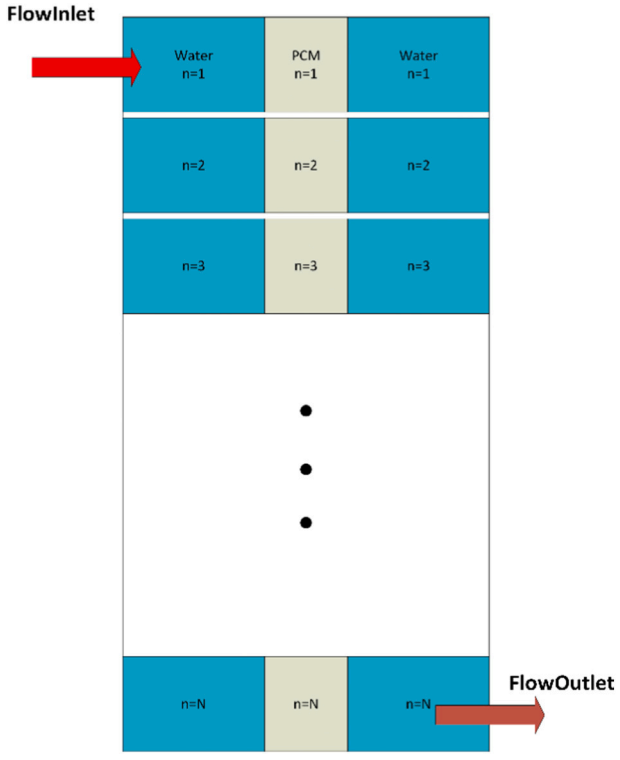

Fig. 1. Schematic diagram of the PCM water energy storage.

The energy differential equation in one dimension for the water tank can be written as Eq. (1). The first term of the left-hand side is the dynamic energy changing term of the layer. The second term represents the flow heat exchange in the form of convection. The first term of the right-hand side describes the conduction heat transfer between adjacent vertical layers. The second term is the heat loss to the ambient air, and the last term represents the heat transfer between water and PCM.

$$\frac{\partial \rho c T_w}{\partial t}+\frac{\partial \rho c u T_w}{\partial x}=\frac{\partial}{\partial x}\left(k\frac{\partial T_w}{\partial x}\right)+h_{hl}A_s(T_a-T_w)\Big/V+\Gamma A_{pw}(T_p-T_w)\Big/V \tag{1}$$

The unsteady differential equation Eq. (1) can be discrete into the all-implicit format by the finite difference method [28] as shown in Eq. (2) by integrating the volume of the water layer. The all-implicit method means that only the initial temperature of the current layer is known in one time step. Other temperatures are unknown final temperatures in the time step.

$$mc\frac{T_i-T_i^0}{\Delta t}=kA_c\frac{T_{i-1}-T_i}{\Delta x}+kA_c\frac{T_{i+1}-T_i}{\Delta x}+\dot{m}c(T_{i-1}-T_i)+h_{hl}A_s(T_a-T_i)+\Gamma A_{pw}(T_{pi}-T_i) \tag{2}$$

By sorting out the terms, Eq. (2) is rewritten as Eq. (3). Three adjacent temperature nodes are arranged on the left-hand side of the equation together with their coefficients, and the other terms are put on the right-hand side, which is typically referred to as the source term.

$$\left(-\frac{kA_c}{\Delta x}-\dot{m}c\right)T_{i-1}+\left(\frac{mc}{\Delta t}+\frac{2kA_c}{\Delta x}+h_{hl}A_s+\dot{m}c+\Gamma A_{pw}\right)T_i+\left(-\frac{kA_c}{\Delta x}\right)T_{i+1}=h_{hl}A_sT_a+\Gamma A_{pw}T_{pi}+\frac{mc}{\Delta t}T_i^0 \tag{3}$$

To illustrate the algebraic equation set, Eq. (3) is simplified into Eq. (4), which uses the coefficient matrix a, b, c, and d to represent the three temperatures' coefficient terms and the source term. If the energy storage is divided into 5 layers, Eq. (4) can be expanded as Eq. (5).

$$aT_{i-1}+bT_i+cT_{i+1}=d \tag{4}$$

$$\begin{bmatrix} b_1 & c_1 & 0 & 0 & 0 \\ a_2 & b_2 & c_2 & 0 & 0 \\ 0 & a_3 & b_3 & c_3 & 0 \\ 0 & 0 & a_4 & b_4 & c_4 \\ 0 & 0 & 0 & a_5 & b_5 \end{bmatrix}\begin{bmatrix} d_1 \\ d_2 \\ d_3 \\ d_4 \\ d_5 \end{bmatrix} \tag{5}$$

The discrete algebraic equation set has the same tridiagonal coefficient matrix as Eq. (5), showing for all the one-dimension energy equations. The Tridiagonal Matrix Algorithm (TDMA) [29] is a classic fast method to solve the algebraic equation set.

The initial temperatures of the tank, the inlet temperature, the flow rate, and the ambient temperature can be set by users as the initial condition.

The boundary condition for the top and bottom nodes can be described by the adiabatic condition like Eq. (6) shows. For the first layer node, the first term temperature T_0 can be assumed equal to the first node temperature T_1. Similarly, for the last layer node, T_{N+1} is assumed as T_N. Alternatively, the boundary condition can also be described by the heat convection equation using the user-provided top/bottom heat loss coefficients. The theory is explained in Section 3.1 and the equations are shown in Eqs. (26) and (27).

The water region model can also be used to simulate a single water tank when the heat transfer term between PCM and water is removed.

$$\begin{aligned}
&\left(-\frac{kA_c}{\Delta x}\right)T_1+\left(\frac{mc}{\Delta t}+\frac{2kA_c}{\Delta x}+h_{hl}A_s+\dot{m}c+\Gamma A_{pw}\right)T_1+\left(-\frac{kA_c}{\Delta x}\right)T_2=h_{hl}A_sT_a+\Gamma A_{pw}T_{p1}+\frac{mc}{\Delta t}T_1^0\\
&\left(-\frac{kA_c}{\Delta x}\right)T_{N-1}+\left(\frac{mc}{\Delta t}+\frac{2kA_c}{\Delta x}+h_{hl}A_s+\dot{m}c+\Gamma A_{pw}\right)T_N+\left(-\frac{kA_c}{\Delta x}\right)T_N=h_{hl}A_sT_a+\Gamma A_{pw}T_{pN}+\frac{mc}{\Delta t}T_N^0
\end{aligned} \tag{6}$$

2.2. The PCM region

The same derivation method is applied to the PCM region. The governing equation for the PCM region is created as Eq. (7). The heat loss term is neglected as the PCM region is surrounded by the water region. However, a heat loss could be added easily if necessary. For example, in cases where the top or the bottom PCM layer directly contacts the ambient environment or that the PCM is located at the outer of the energy storage, the heat loss from the PCM region should be considered.

Like Eq. (1), the dynamic term is on the left-hand side of Eq. (7). The first term on the right-hand side describes the heat conduction between adjacent PCM layers. The second term represents the heat transfer between the PCM and the water in the same layer by a given overall heat transfer coefficient Γ, which considers both the heat convection and conduction impact. The overall heat transfer coefficient Γ is influenced by many aspects, such as the heat exchanger shape, the specific material property, and the operating conditions. It can be determined by experiments, detailed CFD investigations, or theoretical heat transfer analysis. In general, when there is heating or cooling flow, the heat convection affects the most for the overall heat transfer coefficient. When the energy storage is on standby, heat conduction is the dominating heat transfer format between water and PCM.

$$\frac{\partial \rho H_p}{\partial t}=\frac{\partial}{\partial x}\left(k\frac{\partial T_P}{\partial x}\right)+\Gamma A_{pw}(T_w-T_p)\Big/V \tag{7}$$

Unlike Eq. (1), the dynamic energy change of Eq. (7) is described by the enthalpy of PCM since its nonlinear energy-temperature relationship. For a typical solid-liquid PCM, the energy-temperature curve can be divided into the solid part, the phase change (melting or solidification), and the liquid part. See the blue line in Fig. 2. In contrast, a typical sensible energy storage material – like water has linear energy–temperature relationship, shown as the red line in the figure. Theoretically, a PCM has a melting point to indicate the phase change temperature. But in reality, the onset and offset temperatures T_{m1}, T_{m2} are typically observed as the start and the end turning point of the phase change period. In a heating course, T_{m1} is the onset temperature, and T_{m2} is the offset temperature, while in a cooling course, the two temperatures are swapped. The energy difference between T_{m1} and T_{m2} is the latent heat stored or released theoretically from the PCM.

Fig. 2 also shows two types of supercooling phenomenon – namely the supercooling degree and stable supercooling, which are illustrated as the orange and purple line in the PCM cooling process. The two supercooling phenomenon is specifically described in Section 3.4 PCM activation mode.

It is widely recognized using Eq. (8) to describe the enthalpy – temperature relation for a solid-liquid PCM [30]. The main assumption is the energy linearization between T_{m1} and T_{m2}, as the green line indicated in Fig. 2. Therefore, the PCM enthalpy between T_{m1} and T_{m2} is the summation of total solid enthalpy and the latent heat enthalpy weighted by the current temperature ratio $(T-T_{m1})/(T_{m1}-T_{m2})$. The temperature ratio can also evaluate how much PCM is currently melted. Therefore, it is also well known as the PCM melting fraction.

$$H_p=\begin{cases} c_sT & T<T_{m1}\\ c_sT_{m1}+\dfrac{E_L(T-T_{m1})}{T_{m2}-T_{m1}} & T_{m1}\le T\le T_{m2}\\ c_sT_{m1}+E_L+c_l(T-T_{m2}) & T>T_{m2}\end{cases} \tag{8}$$

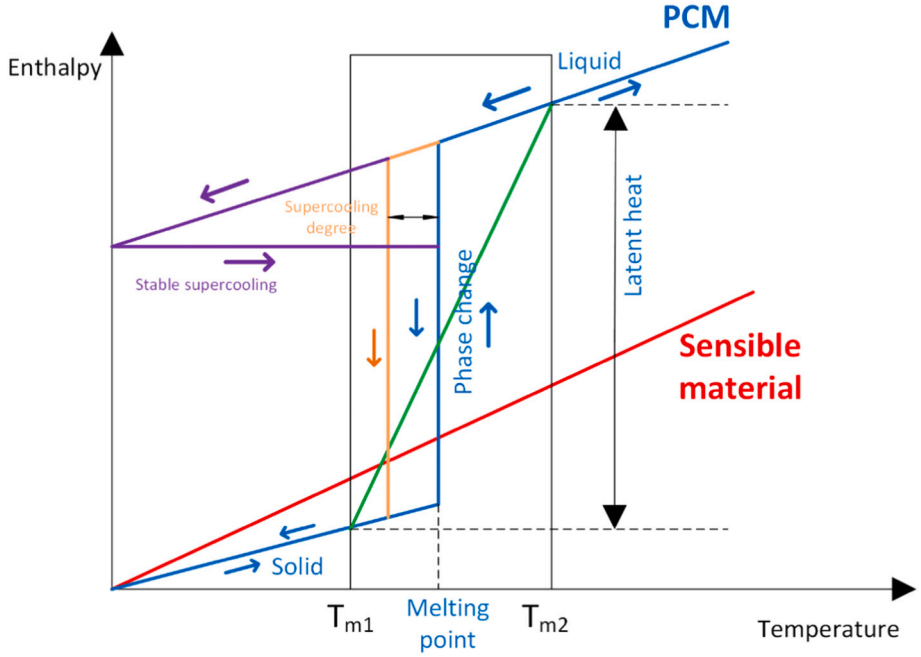

Fig. 2. Schematic diagram of enthalpy temperature profile for sensible and phase change materials. (For interpretation of the references to colour in this figure, the reader is referred to the web version of this article.)

It is natural to convert the enthalpy term into the temperature term by a linear relation, as shown in Eq. (9) according to Fig. 2. Then the enthalpy at different temperatures can be substituted by the temperature with its coefficients S_1 and S_2. Of course, S_1 and S_2 have specific expressions in the PCM solid phase, the melting/solidification phase, and the liquid phase, shown in Eq. (10).

$$H_p = S_1 T + S_2 \tag{9}$$

$$\begin{cases} S_{1a} = c_s, S_{2a} = 0 & T \le T_{m1} \\ S_{1b} = \dfrac{E_L}{T_{m2} - T_{m1}}, S_{2b} = c_s T_{m1} - \dfrac{E_L T_{m1}}{T_{m2} - T_{m1}} & T_{m1} < T \le T_{m2} \\ S_{1c} = c_l, S_{2c} = E_L + c_s T_{m1} - c_l T_{m2} & T > T_{m2} \end{cases} \tag{10}$$

The enthalpy term can be discrete into the initial and end temperature terms with their specific S_1 and S_2 coefficients, as shown in Eq. (11). Then the PCM enthalpy governing equation is converted into the typical temperatures equation as Eq. (12).

$$m\frac{S_1 T_p + S_2}{\Delta t} - m\frac{S_1^0 T_p^0 + S_2^0}{\Delta t} = V\frac{\partial}{\partial x}\left(k\frac{\partial T_p}{\partial x}\right) + \Gamma A_{pw}\left(T_w - T_p\right) \tag{11}$$

$$m\frac{S_1 T_p}{\Delta t} = V\frac{\partial}{\partial x}\left(k\frac{\partial T_p}{\partial x}\right) + \Gamma A_{pw}\left(T_w - T_p\right) + m\frac{S_1^0 T_p^0 + S_2^0 - S_2}{\Delta t} \tag{12}$$

Eq. (12) is further discrete for the heat conduction term as Eq. (13). Finally, the three nodes format discrete equation is sorted into Eq. (14), which can be simplified the same as Eq. (4) with the corresponding a, b, c, d coefficients listed in Eq. (15).

$$m\frac{S_1 T_i}{\Delta t} = kA_c\frac{T_{i-1} - T_i}{\Delta x} + kA_c\frac{T_{i+1} - T_i}{\Delta x} + \Gamma A_{pw}(T_w - T_i) + m\frac{S_1^0 T^0 + S_2^0 - S_2}{\Delta t} \tag{13}$$

$$\begin{aligned} &-\frac{kA_c}{\Delta x}T_{i-1} + \left(\frac{mS_1}{\Delta t} + \frac{2kA_c}{\Delta x} + \Gamma A_{pw}\right)T_i - \frac{kA_c}{\Delta x}T_{i+1} \\ &= \Gamma A_{pw} T_w + m\frac{S_1^0 T^0 + S_2^0 - S_2}{\Delta t} \end{aligned} \tag{14}$$

$$\begin{aligned} a &= c = -\frac{kA_c}{\Delta x} \\ b &= \frac{mS_1}{\Delta t} + \frac{2kA_c}{\Delta x} + \Gamma A_{pw} \\ d &= \Gamma A_{pw} T_w + m\frac{S_1^0 T^0 + S_2^0 - S_2}{\Delta t} \end{aligned} \tag{15}$$

$$(m_w c_w + m_t c_t)\frac{T_i - T_i^0}{\Delta t} = kA_c\frac{T_{i-1} - T_i}{\Delta x} + kA_c\frac{T_{i+1} - T_i}{\Delta x} + \dot{m}c(T_{i-1} - T_i) + h_{hl}A_s(T_a - T_i) + \Gamma A_{pw}\left(T_{pi} - T_i\right) \tag{16}$$

2.3. The PCM water energy storage and the iteration method

The final aim of this work is to develop a mathematical model of energy storage containing both PCM and water. The model can calculate the status of both materials at any time during the operating period.

Take the PCM water energy storage shown in Fig. 1 as an example. The water is outside of the PCM. The governing equation for the water tank is Eq. (1) and the governing equation for the PCM region is Eq. (7). An iteration method is developed to derive the correct temperatures for both water and PCM at any time step. It is convenient to use $Tw(T_{wo},T_{po})$ and $Tp(T_{wo},T_{po})$ to represent the water and PCM governing equations. The final water temperature Tw and the final PCM temperature Tp can be derived if the initial and boundary conditions are given. In one time step, the iteration is carried out in the following steps:

Step 1: The first water temperature T_{w1} is obtained from the water governing equation $Tw(T_{wo},T_{po})$ by giving the initial water temperature T_{wo} and the initial PCM temperatures T_{po}. This process can be represented by $T_{w1} = Tw(T_{wo},T_{po})$. Then use the initial PCM temperature T_{p0} and the new water temperature T_{w1} as the initial temperatures for the PCM governing equation. The first PCM temperature T_{p1} is derived by $T_{p1} = Tp(T_{w1},T_{po})$.

Step 2: The second water temperature T_{w2} is calculated by giving the initial water temperature and the updated PCM temperature T_{p1} through $T_{w2} = Tw(T_{wo},T_{p1})$. Like step 1, the second PCM temperature is derived by giving the initial PCM temperature T_{p0} and the updated water temperature T_{w2} through $T_{p2} = Tp(T_{w2}, T_{po})$.

The steps are calculated continuously until the difference of the water and PCM temperatures in two steps is extremely small. For example, the temperature difference is less than 10^{-6} K. Then, the iteration is converged, and the final water and PCM temperatures are derived for the time step.

2.4. Considering the sensible heat content of other tank materials in the energy storage

The tank material of the energy storage consists typically of a metallic structure that forms the storage frame and the inside heat exchanger. The sensible heat of these materials should be considered in the calculation. One possible method is to create separate governing equations for the inside heat exchanger and the tank walls, like the water and PCM part in Sections 2.1 and 2.2, using the same discrete method for the two extra equations. Then apply the iteration method for the four equations to achieve converged temperature results of the water, PCM, inside heat exchanger, and the tank walls. However, the method will cost extra calculation resources, and the tank wall or tube shell temperatures are not so important. Therefore, a simple method is applied by assuming that the metallic structure has the same temperature as the water in each layer since the heat transfer between water and the metallic structure is better than that between PCM and the metallic structure. A further assumption is that the volume of the metallic structure is neglected. Then the mass and heat capacity of the metallic structure is added to the dynamic term of the water governing equation, shown in Eq. (16).

It may happen in some cases that the water is inside of the heat exchanger while the PCM is outside and directly contacts the tank walls. In this situation, the inside heat exchanger can be assumed to have the same temperature as the water, while the temperature of the tank walls cannot. If considering the tank walls have the same temperature as PCM, theoretically, it may cause errors due to the contact thermal resistance in the dynamic charging and discharging process until stable conditions are reached. Users may try the simple method first. If the result errors are within reasonable limits compared to measured results, the simple method can be used. Otherwise, it is recommended to develop the third governing equation for the tank walls and follow the same solving method and iteration method for the equation set.

2.5. Energy balance check

Energy balance check after each time step is a crucial method to guarantee the correctness of the calculation. The technique was used in all the simulations in this work.

Eq. (17) is the energy balance equation for the PCM water energy storage. The energy balance error is calculated by Eq. (18). Q_{in} refers the input power to the energy storage while Q_{loss} is the heat losses to the environment. Q_{Aux} is the auxiliary power input. ΔQ_{water} and ΔQ_{PCM} are the water or PCM energy change during one time step. dQ is the power difference of the terms mentioned above, while Er is the power balance error. Since all the powers are calculated for one time step, we follow the routine of calling the power balance check as energy balance check. Some terms can be removed from Eq. (17) for a single material energy storage or in some specific operating conditions. For example, when a single PCM energy storage is in standby status, Q_{in}, Q_{Aux}, and ΔQ_{water} are 0. The energy flows can hardly be completely balanced since the numerical method usually cause calculation errors. However, the energy balance error is a good indicator for users to check the logic and the calculation of the numerical method.

$$dQ = Q_{in} + Q_{loss} + Q_{Aux} - \Delta Q_{water} - \Delta Q_{pcm} \tag{17}$$

$$Er = \frac{dQ}{Q_{in} + Q_{Aux} + Q_{loss}} \tag{18}$$

2.6. The particular time steps of PCM temperature across the melting points

Using the energy balance check, the authors found that the PCM temperatures could not be calculated correctly by the method described in Sections 2.2 and 2.3 in some particular time steps when the PCM temperature crosses the melting points. The reason is, for the PCM heating or cooling process, most of the time steps are usually in one of the three PCM statuses – either solid, melting/solidification, or liquid. Therefore, a constant S_1 and S_2 set can be correctly assigned for those time steps, and the energy balance error is small. However, when the time steps cross the melting points – either T_{m1} or T_{m2} – there exists two PCM statuses in one time step. The S_1 and S_2 set must be changed during the time step.

Take a heating time step as an example. See Fig. 3. In one time step Δt, the initial PCM temperature T_0 is below T_{m1} while the end temperature T_1 is higher than T_{m1}. Therefore, during the sub time step Δt_1, PCM is solid, and the S_1 and S_2 are S_{1a} and S_{2a}, while in Δt_2, PCM is partly melted, so S_1 and S_2 should be S_{1b} and S_{2b}.

The solution for those special time steps is to create two separate Eq. (11) with their corresponding sub time step. As Fig. 3 shows, Eq. (19) is the governing equation for sub time step Δt_1 in the discrete format. Since the initial and final temperatures in Δt_1 are known, Δt_1 can be calculated from Eq. (20). Then Δt_2 is derived by Eq. (21). In the sub time step Δt_2, Eq. (22) is the governing equation with the correct S_1 and S_2. By combining Eqs. (20) and (22), Eq. (23) is derived, which is the correct governing equation for the whole time step Δt, and Eq. (24) is the final sorted format.

There are in total four cases that need special treatment - the heating time steps cross T_{m1} and T_{m2}, and the cooling time steps cross over T_{m2} and T_{m1}.

$$m\frac{S_{1a}T_{m1} + S_{2a}}{\Delta t_1} = kA_c\frac{T_{i-1,m} - T_{m1}}{\Delta x} + kA_c\frac{T_{i+1,m} - T_{m1}}{\Delta x} + \Gamma A_{pw}(T_w - T_{m1}) + m\frac{S_{1a}T^0 - S_{2a}}{\Delta t_1} \tag{19}$$

$$\Delta t_1 = \frac{mS_{1a}\left(T_{m1} - T^0\right)}{\frac{kA_c}{\Delta x}\left(T_{i-1,m} + T_{i+1,m} - 2T_{m1}\right) + \Gamma A_{pw}(T_w - T_{m1})} \tag{20}$$

$$\Delta t_2 = \Delta t - \Delta t_1 \tag{21}$$

$$m\frac{S_{1b}T_i}{\Delta t_2} = kA_c\frac{T_{i-1} - T_i}{\Delta x} + kA_c\frac{T_{i+1} - T_i}{\Delta x} + \Gamma A_{pw}(T_w - T_i) + m\frac{S_{1a}T_{m1} + S_{2a} - S_{2b}}{\Delta t_2} \tag{22}$$

$$m\frac{S_{1a}T_{m1}}{\Delta t_1} + m\frac{S_{1b}T_i}{\Delta t_2} = kA_c\frac{T_{i-1} + T_{i-1,m} - T_{m1} - T_i}{\Delta x} + kA_c\frac{T_{i+1} + T_{i+1,m} - T_{m1} - T_i}{\Delta x} + \Gamma A_{pw}(2T_w - T_{m1} - T_i) + m\frac{S_{1a}T^0}{\Delta t_1} + m\frac{S_{1a}T_{m1} - S_{2b}}{\Delta t_2} \tag{23}$$

$$-\frac{kA_c}{\Delta x}T_{i-1} + \left(\frac{mS_{1b}}{\Delta t_2} + \frac{2kA_c}{\Delta x} + \Gamma A_{pw}\right)T_i - \frac{kA_c}{\Delta x}T_{i+1} = \frac{kA_c}{\Delta x}\left(T_{i-1,m} + T_{i+1,m} - 2T_{m1}\right) + 2\Gamma A_{pw}T_w - \Gamma A_{pw}T_{m1} + m\frac{S_{1a}\left(T^0 - T_{m1}\right)}{\Delta t_1} + m\frac{S_{1a}T_{m1} - S_{2b}}{\Delta t_2} \tag{24}$$

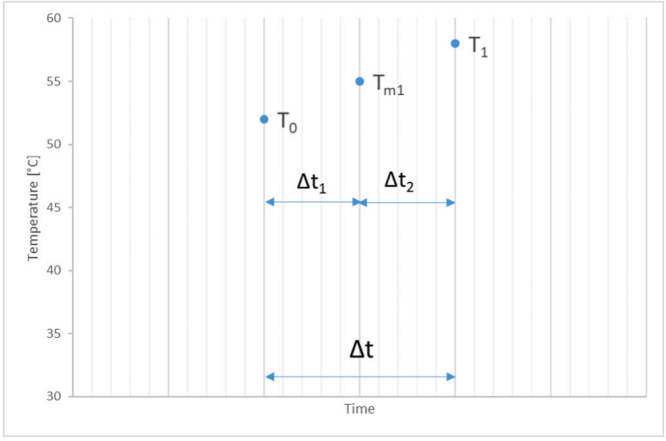

Fig. 3. An example of one time step that crosses over T_{m1} melting point.

It should be noted that the correct upper and lower layer temperatures of the PCM are still unknown during the calculation. In order to calculate the heat conduction effect, it is assumed to use the mean temperatures of the upper ($T_{i-1,m}$) and lower PCM layer ($T_{i+1,m}$) to substitute the final temperatures in the calculation. The assumption will increase the numerical error. The energy balance check also shows that in those special time steps, the error is usually higher than in other time steps. But the errors are within reasonable scientific scope, for example, 5 %, so it is accepted.

3. Extended functionality development

For simplicity, the mathematical model was derived and solved by its simplest prototype form in Section 2. The prototype was modeled with the adiabatic boundary condition for the top and bottom nodes, with a uniform heat loss coefficient, with a fixed flow inlet on the top layer and a fixed flow outlet at the bottom layer. The prototype did not consider

modeling an auxiliary heater and natural convection in the water tank. In this section, the additional functionality is developed by directly modifying the mathematical model without new assumptions introduced.

3.1. Separate heat loss coefficients and auxiliary heater

The uneven heat loss coefficients can be easily modeled for the outer tank, regardless of a water tank or a PCM tank. For example, users can assign a specific heat loss coefficient for each layer at side h_{hl_i}, a top heat loss coefficient h_{hl_top}, and a bottom heat loss coefficient h_{hl_bot}. Take a water tank as an example. Eq. (3) with a uniform side heat loss coefficient became Eq. (25) with specific side heat losses coefficients. Further, if the heat convection boundary condition is required, the top and bottom heat loss terms need to be added, as Eqs. (26) and (27) shown.

One or multi auxiliary heaters in specific layers can be easily added. Q_{Aux_i} represents the power of the auxiliary heater, and it only needs to be added in the source terms at the right-hand side of the equation.

$$\left(-\frac{kA_c}{\Delta x}-\dot{m}c\right)T_{i-1}+\left(\frac{mc}{\Delta t}+\frac{2kA_c}{\Delta x}+h_{hl\_i}A_s+\dot{m}c+\Gamma A_{pw}\right)T_i+\left(-\frac{kA_c}{\Delta x}\right)T_{i+1} = h_{hl\_i}A_sT_a+\Gamma A_{pw}T_{pi}+\frac{mc}{\Delta t}T_i^0+Q_{Aux\_i} \tag{25}$$

$$\left(\frac{mc}{\Delta t}+\frac{2kA_c}{\Delta x}+h_{hl\_1}A_s+h_{hl\_top}A_c+\dot{m}c+\Gamma A_{pw}\right)T_1+\left(-\frac{kA_c}{\Delta x}\right)T_2 = h_{hl\_1}A_sT_a+h_{hl\_top}A_cT_a+\Gamma A_{pw}T_{p1}+\frac{mc}{\Delta t}T_1^0+Q_{Aux\_1} \tag{26}$$

$$\left(-\frac{kA_c}{\Delta x}-\dot{m}c\right)T_{N-1}+\left(\frac{mc}{\Delta t}+\frac{2kA_c}{\Delta x}+h_{hl\_N}A_s+h_{hl\_bot}A_c+\dot{m}c+\Gamma A_{pw}\right)T_N = h_{hl\_N}A_sT_a+h_{hl\_bot}A_cT_a+\Gamma A_{pw}T_{pN}+\frac{mc}{\Delta t}T_N^0+Q_{Aux\_N} \tag{27}$$

3.2. Flexible inlet and outlet layers

In order to model a water tank with flexible inlet and outlet positions, three coefficient lists α, β, and γ are specified, indicating whether there is flow or not in each layer and the flow direction. The three lists can only contain the same amount of 0 or 1 as the total number of layers. α represents the flow from top to bottom while β is the opposite. See Eqs. (28) and (29).

Take a five layers water tank as an example. The inlet flow enters at layer 2 and exits at layer 4. Therefore, there are flows in layer 2, 3 and 4. The three lists are then assigned as α = [0,0,1,1,0], β = [0,0,0,0,0] and γ = [0,1,1,1,0].

$$mc\frac{T_i-T_i^0}{\Delta t}=kA_c\frac{T_{i-1}-T_i}{\Delta x}+kA_c\frac{T_{i+1}-T_i}{\Delta x}+\alpha\dot{m}c(T_{i-1}-T_i)+\beta\dot{m}c(T_{i+1}-T_i)+h_{hl}A_s(T_a-T_i)+\Gamma A_{pw}(T_{pi}-T_i) \tag{28}$$

$$\left(-\frac{kA_c}{\Delta x}-\alpha\dot{m}c\right)T_{i-1}+\left(\frac{mc}{\Delta t}+\frac{2kA_c}{\Delta x}+h_{hl}A_s+\gamma\dot{m}c+\Gamma A_{pw}\right)T_i+\left(-\frac{kA_c}{\Delta x}-\beta\dot{m}c\right)T_{i+1}=h_{hl}A_sT_a+\Gamma A_{pw}T_{pi}+\frac{mc}{\Delta t}T_i^0 \tag{29}$$

3.3. Mixing effect in the water tank

In the water tank, the mixing effect is caused by the thermally unstable condition of layers temperature – a layer temperature is higher than the layer above. The natural convection will automatically form an opposite thermal-driven force to decrease the temperature difference. Two typical methods can be used to model the mixing effect in the water tank [31]. One is the complete mixing method. If the unstable layers are found at the end of one time step, the two layer temperatures are averaged, and the mean temperature is assigned as the end temperatures for the two layers. The complete mixing method is equivalent to an infinite reverse flow in two layers. The method is straightforward and is widely used.

The other option is providing a user-defined reverse flow rate. Eq. (30) is the mathematical model for this method. Two additional terms with the reverse flow mix and its coefficient list f_1, f_2 are added to the discrete equation. f_1 and f_2 are the coefficients to determine whether

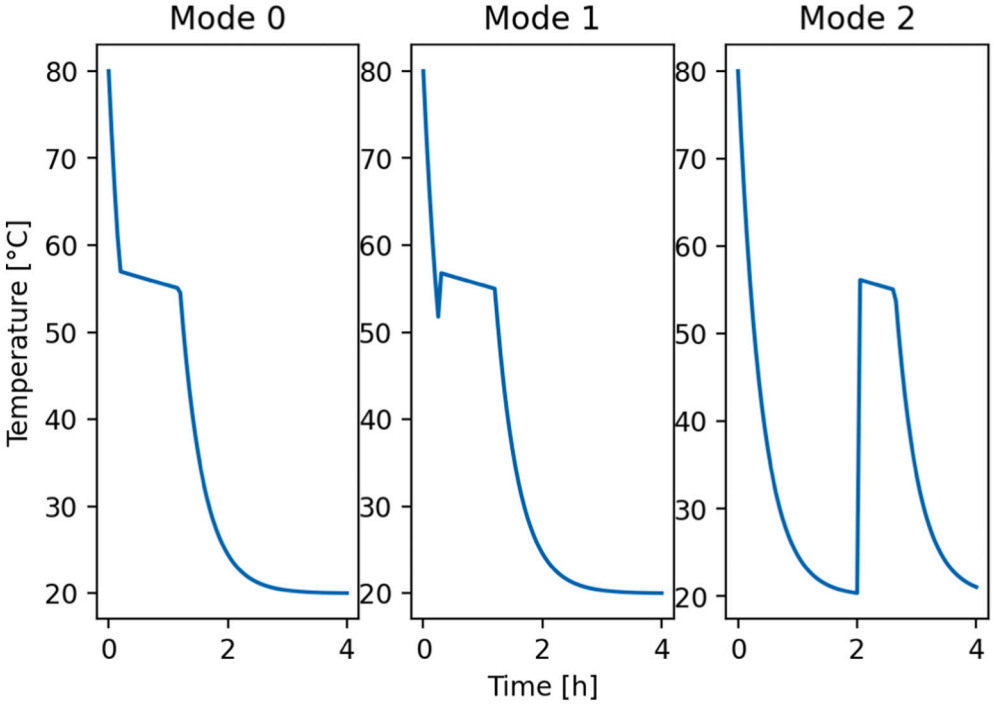

Fig. 4. PCM cooling process with three supercooling modes: Mode 0, no supercooling; Mode 1, supercooling degree; Mode 2, stable supercooling.

Fig. 5. The PCM water energy storage with (right) and without (left) insulation [34].

there is a reverse flow for the current layer with its upper and lower layers. Unlike the flow coefficients α, β, and γ, f_1 and f_2 must be determined at each time step.

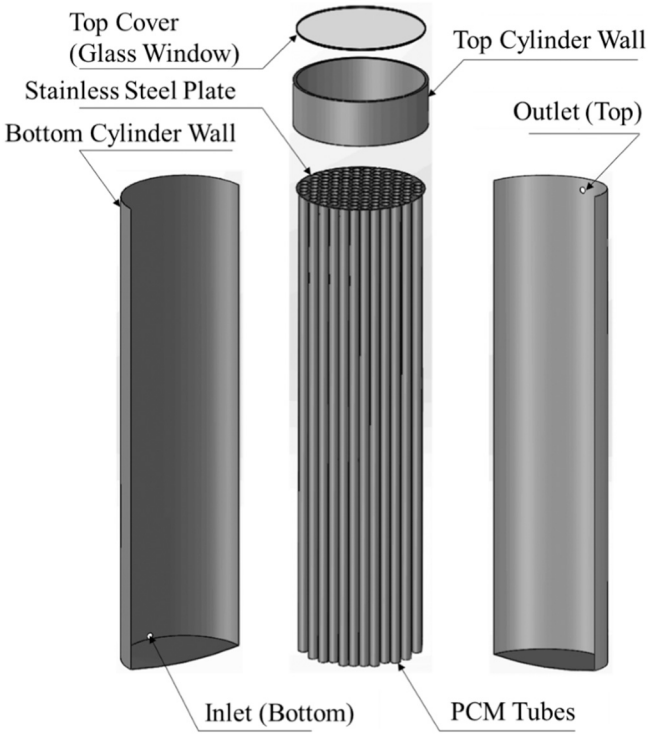

Fig. 6. The break down 3D drawing of the PCM water energy storage [34].

$$mc\frac{T_i - T_i^0}{\Delta t} = kA_c\frac{T_{i-1} - T_i}{\Delta x} + kA_c\frac{T_{i+1} - T_i}{\Delta x} + \dot{m}c(T_{i-1} - T_i) + h_{hl}A_s(T_a - T_i) + f_1\dot{m}_{mix}c(T_{i-1} - T_i) + f_2\dot{m}_{mix}c(T_{i+1} - T_i) \quad (30)$$

3.4. PCM activation mode

Supercooling is a common phenomenon in the PCM cooling process, especially for salt hydrates. There are typically two supercooling modes. One is the so-called supercooling degree. Liquid PCM is cooled below the melting point without solidification until a lower temperature is reached. The difference between the practical solidification temperature and the melting point is the supercooling degree, shown as the orange curve in Fig. 2. The other case is stable supercooling, which means PCM can be cooled to the ambient temperature without solidification and kept in the liquid phase. Solidification can be activated by different nucleation techniques [32]. The temperature of the activated PCM will increase since the latent heat of fusion is released, see the purple curve in Fig. 2.

In the prototype model, no supercooling effect is modeled as mode 0. In a heating process, the solid PCM will start melting at the onset temperature T_{m1} and fully melt at the offset temperature T_{m2}, while in a cooling process, the liquid PCM will start solidification at T_{m2} and become fully solid at T_{m1}. See the first figure in Fig. 4.

The above-mentioned two supercooling modes are developed to the PCM model. The supercooling degree mode is defined as mode 1 in the PCM model and the stable supercooling mode is defined as mode 2. For the supercooling degree mode, users provide the value of supercooling degree. Only T_{m2} in the cooling process needs to be updated by subtracting the supercooling degree. Therefore, when the liquid PCM first reaches or is lower than the new T_{m2}, it will start solidification, and the PCM temperature will increase by releasing the latent heat. See the second figure in Fig. 4, in which the activation starts at hour 0.25.

The stable supercooling mode can be carried out by assigning a very low T_{m2}, lower than the ambient temperature. In that case, the liquid PCM will not start solidification in the cooling process. Users need to give a signal to activate the solidification at a particular time step, or the signal can be sent according to a specific control strategy. When a signal is sent to the PCM model, the S_1 and S_2 set is changed, and the solidification starts. See the third figure in Fig. 4. The PCM was first stably cooled down to ambient temperature. Then the activation signal is sent at hour 2 and then the PCM started solidification.

4. Experimental verification

4.1. Test facility and set up

The experiments were carried out at Technical University of Denmark. The PCM water energy storage is shown in Fig. 5. The total height of the cylinder storage is 1.7 m. The outer diameter is 0.4 m without insulation. There are 112 tubes installed vertically inside the tank, each with a length of 1.52 m and an inner diameter of 0.0276 m, see Fig. 6. The top end of the tubes is fixed to a stainless-steel plate and opens to the enclosed space above, see Fig. 7. The enclosed space tolerates the volume change related to the phase change of the PCM. The top cover is transparent for inspection. Two tubes are connected to the enclosed space through the top cover. One is for balancing the pressure difference between the ambient and the top of the energy storage. The other with a valve is used for activating the solidification process of the stable supercooled PCM by delivering solid PCM powders. The inlet of the storage is placed at the bottom tank side, while the outlet is placed on the opposite tank side at the upper part of the tank. The tank is insulated with 30 mm mineral wool. There are in total 137.8 kg PCM filled into the 112 tubes and 75 l water in the shell outside. The heat transfer area between the PCM and water is 16.2 m^2. The energy storage

Fig. 7. The manifold plate with a top view of the tubes inside the storage (PCM was melted) [34].

Table 1
The PCM thermal properties used in the simulation [34].

Properties	Values	Units
Melting temperature range	53–54	°C
Latent heat of fusion	209	kJ/kg
Specific heat capacity_solid	2800	J/(kg·K)
Specific heat capacity_liquid	3100	J/(kg·K)
Density_solid	1300	kg/m^3
Density_liquid	1280	kg/m^3
Thermal conductivity	0.5	W/(m·K)

main structure is made of 166 kg stainless steel [33,34].

The PCM used in the experiments was a SAT (sodium acetate trihydrate) based composite with liquid polymer and extra water, developed by HM Heizkörper GmbH Heating Technology [35]. The thermal properties of the PCM used in the simulation are listed in Table 1.

The schematic diagram of the test rig is shown in Fig. 8. The water flow is pumped into the tank bottom and flows out through the outlet on the top. The heating and cooling units can adjust the water temperature before entering the tank. Ten thermocouple sensors are attached to the tank's outer surface with good thermal contact and are covered by the insulation. There are also temperature measurements at the inlet and outlet locations and for the ambient environment. The water flow rate is measured by the flow meter. According to the separate heat loss experiments, a uniform heat loss coefficient of 3.6 W/K was used in the simulation.

A complete test sequence was carried out from 5 June to 8 June 2019. The test lasted for 73 h, including the charging, the sensible heat discharging, the activation of PCM solidification, and the latent heat discharging periods. The inlet, outlet, and ambient temperatures during the complete test course are shown in Fig. 9. The flow rate was kept at 7 l/min during the whole test. All the measured parameters were recorded by a data logger with a data log interval of 1 min.

The first 4.6 h of the test was a preparation period to make sure the initial temperature of the whole storage was uniform at around 30 °C. Then the inlet temperature was set to 92 °C to charge the PCM water energy storage. The charging period lasted about 20 h to guarantee the PCM inside the tank was fully melted. At hour 25, the inlet temperature was set back to 30 °C to start the discharging of the energy storage. Since the PCM was stably supercooled during the discharging, only the sensible heat of water and PCM was discharged. At hour 49, the PCM inside the tank was activated to start solidification by dropping PCM crystals through the delivering tube on the tank top. Then the energy storage temperature increased, and the latent heat was released and discharged afterward.

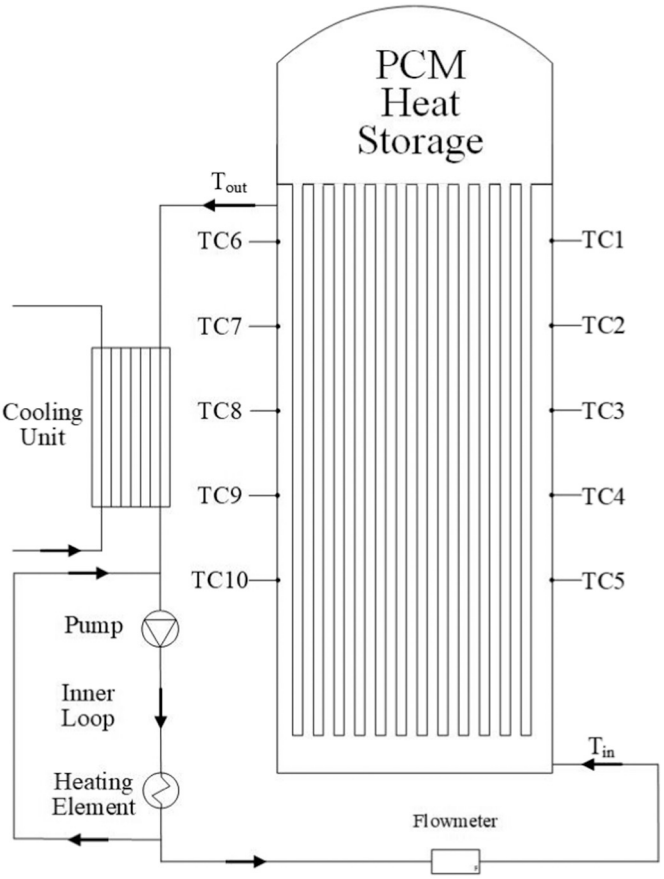

Fig. 8. Schematic diagram of the test facility with the PCM water energy storage [33].

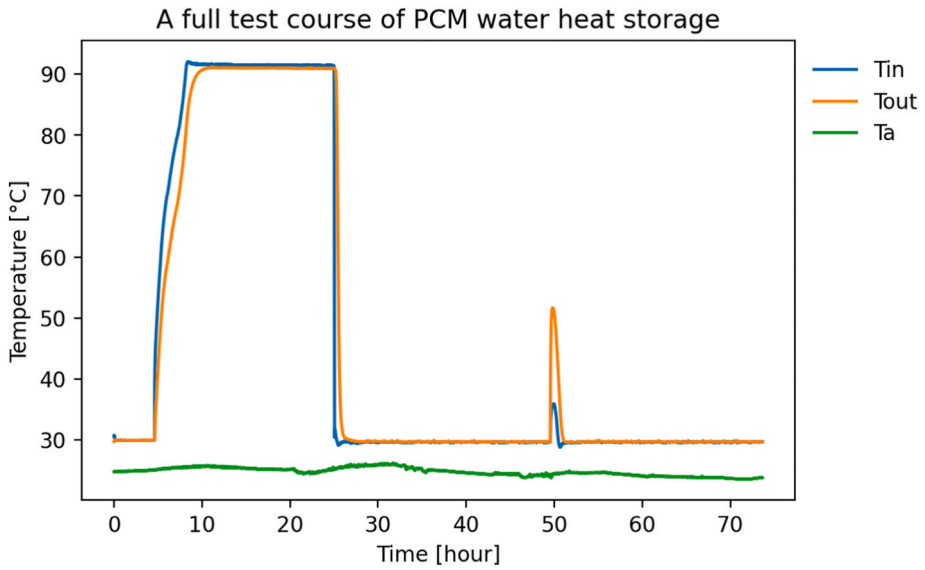

Fig. 9. A full test course of the PCM water energy storage.

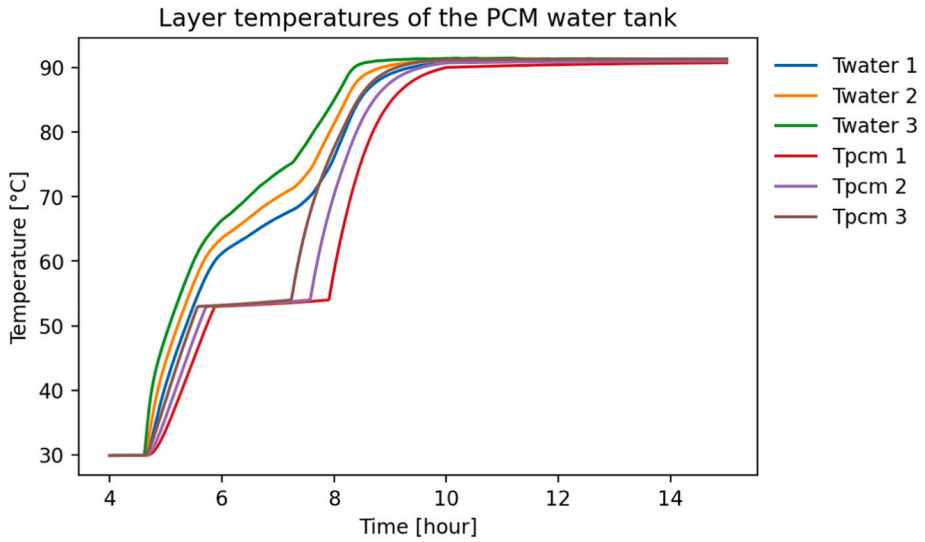

Fig. 10. Simulated layer temperatures of the PCM water tank in the heating period.

4.2. Simulation and results

The PCM water energy storage was numerically modeled, as Fig. 1 shows. The numerical tank was divided into three layers. The inlet is at the 3rd layer, and the outlet is at the 1st layer. The height of the tank is set to 1.52 m since it is the height of the PCM vertical tube, which is the main heat transfer area between the water and the PCM. The material thermal properties and other dimensions follow the experiments' practical values. The overall heat transfer coefficient between water and PCM is theoretically calculated and estimated based on the tank's design, the layout of the inside heat exchangers, and the mean temperature of the energy storage. The calculation method is discussed in Section 5.2. The parameter is affected by many factors and always changing. Therefore, using a constant parameter is not the best estimation. However, the derivation of a constant parameter is much simpler compared to the real-time changing calculation, and the simulation results are good enough. Therefore, the parameter was just calculated for the three periods and set at 100 W/K in the charging period, 600 W/K in the sensible heat discharging period, and 550 W/K in the latent heat discharging period. The time step of the simulation is also assigned as 1 min.

The simulation results, the outlet temperature comparison, and the energy balance error are shown separately for the charging period, the sensible heat discharging period and the latent heat discharging periods in Figs. 10–18. Fig. 19 shows the comparison of the experimental and simulated heat content development during the full test period, and Table 2 summarizes the total charged and discharged heat for the three periods.

Figs. 10, 13, and 16 illustrate calculations of the layer temperature development of the water and PCM in the three periods. Thermal stratification was formed. During charging, the water temperatures were higher than the PCM temperatures, and the top temperatures were lower than the bottom temperatures since the inlet flow was from the bottom. The PCM temperature curves developed as expected in the solid, melting, and liquid phases. The PCM melting started at 53 °C and ended at 54 °C. It can be seen clearly that the water temperatures were influenced by the PCM temperatures, especially in the PCM melting period. Fig. 13 shows the layer temperatures in the sensible heat discharging period. The PCM temperatures developed similar to the water temperature in the same layer because the PCM was kept ideally as the liquid

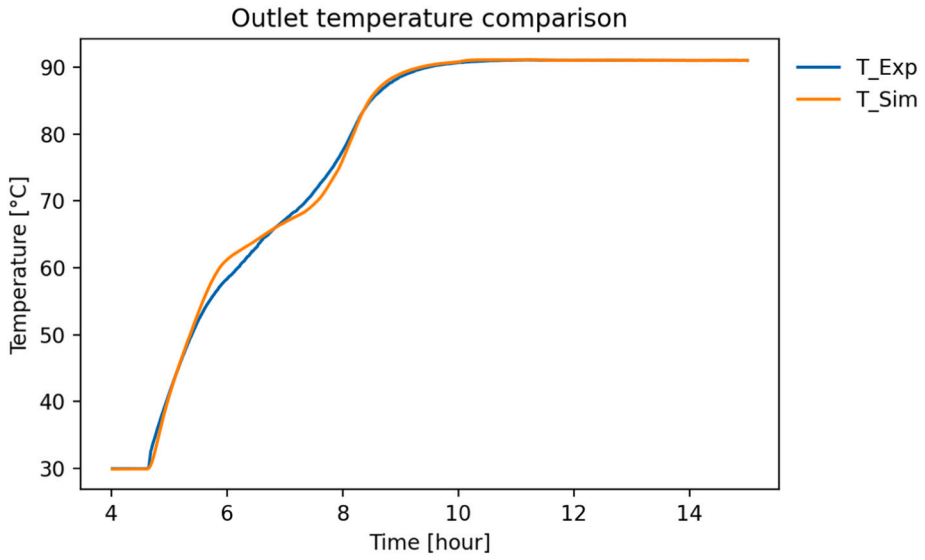

Fig. 11. Experimental and simulated outlet temperature comparison in the heating period.

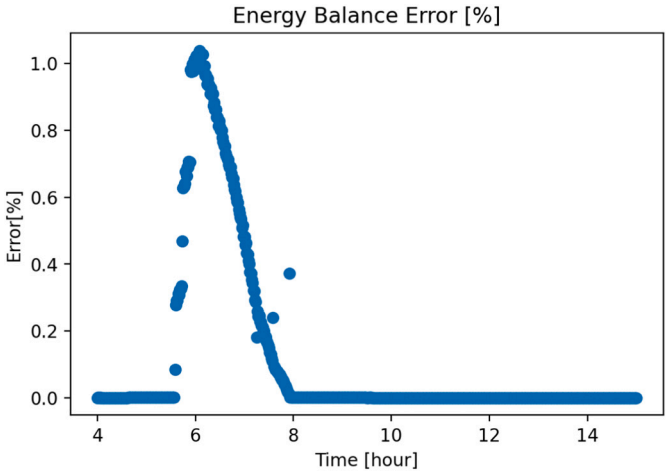

Fig. 12. Energy balance error in the heating period.

phase in the stable supercooling status even its temperature decreased lower than the melting temperature. Fig. 16 shows the development of the temperature in the latent heat discharging period. At hour 49.7, the PCM was activated to start solidification. Then the PCM temperatures rise immediately and transfer heat to the water simultaneously. The PCM did not reach the highest melting temperature of 54 °C because it started solidification from 29.5 °C, and then the released energy was transferred to heat the water and raise its own. The water was heated by the PCM and cooled by the inlet flow. The water top layer temperature reached the highest of 51.7 °C.

Figs. 11, 14, and 17 show comparisons between the calculated and measured outlet temperatures. It can be seen from the figures that all the simulated results can follow the trend of the experimental measurements. The simulated outlet temperature in the heating and solidification period fits quite well with the measured. The maximum deviation is 2.9 K and 2.6 K, separately while the relative errors are 5 % and 6.4 %. The significant difference occurred in Fig. 14 in the sensible heat discharging period. The simulated temperature started to decrease faster than the measured in the first half of the period and then slower in the second half. The reason is that the 3 layers numerical model is too rough to simulate the mixing flow with a large temperature difference between

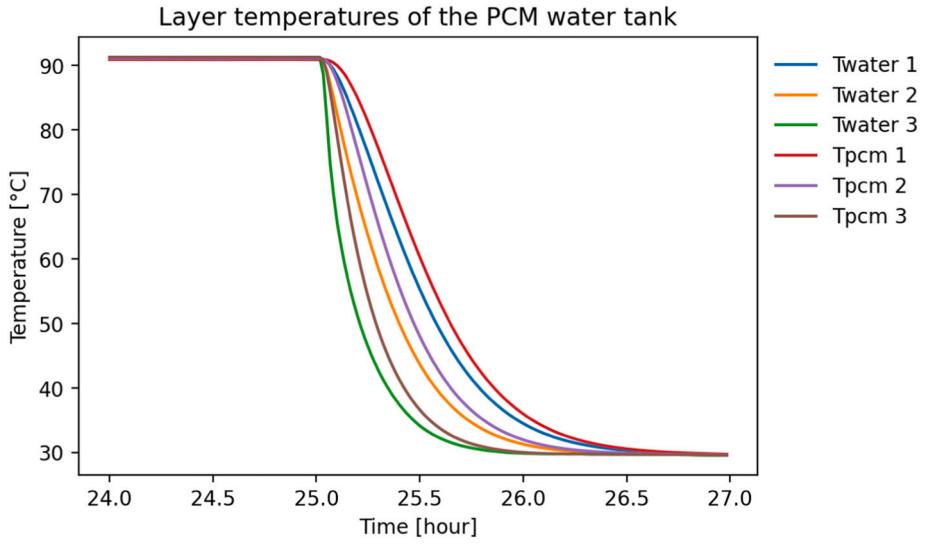

Fig. 13. Simulated layer temperatures of the PCM water tank in the sensible heat discharging period.

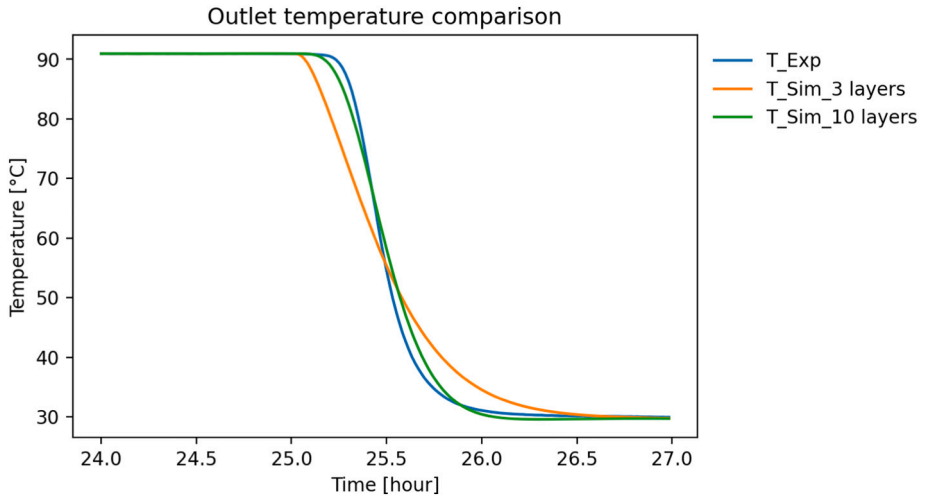

Fig. 14. Experimental and simulated outlet temperature comparison in the sensible heat discharging period. (For interpretation of the references to colour in this figure, the reader is referred to the web version of this article.)

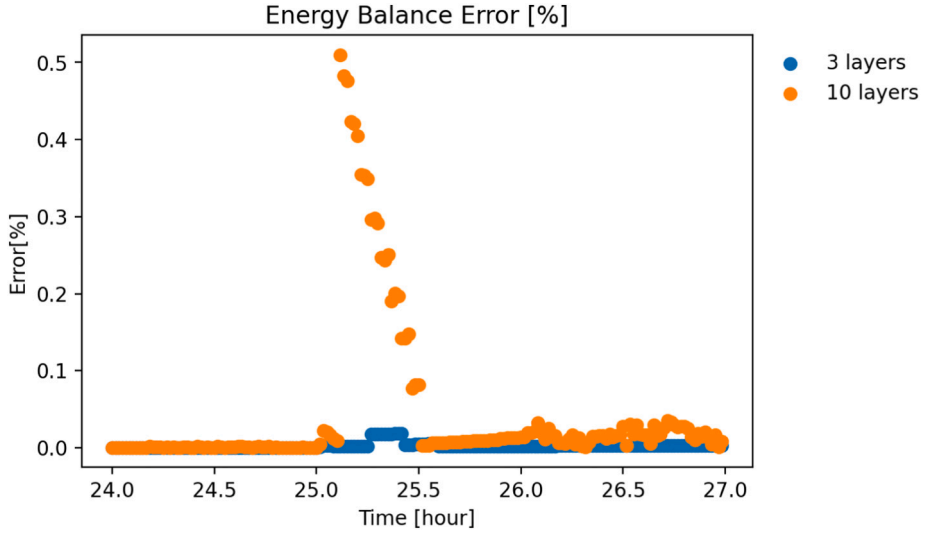

Fig. 15. Energy balance error in the sensible heat discharging period.

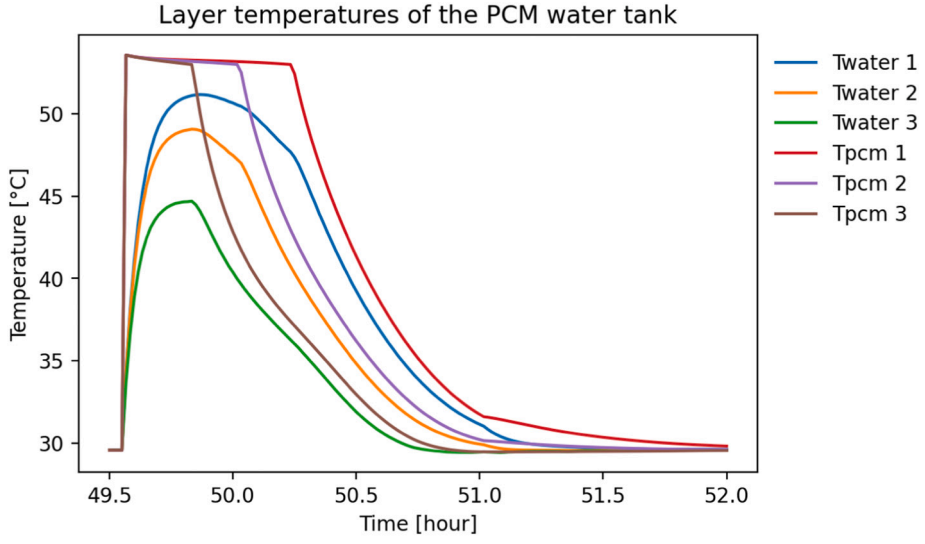

Fig. 16. Simulated layer temperatures of the PCM water tank in the PCM solidification period.

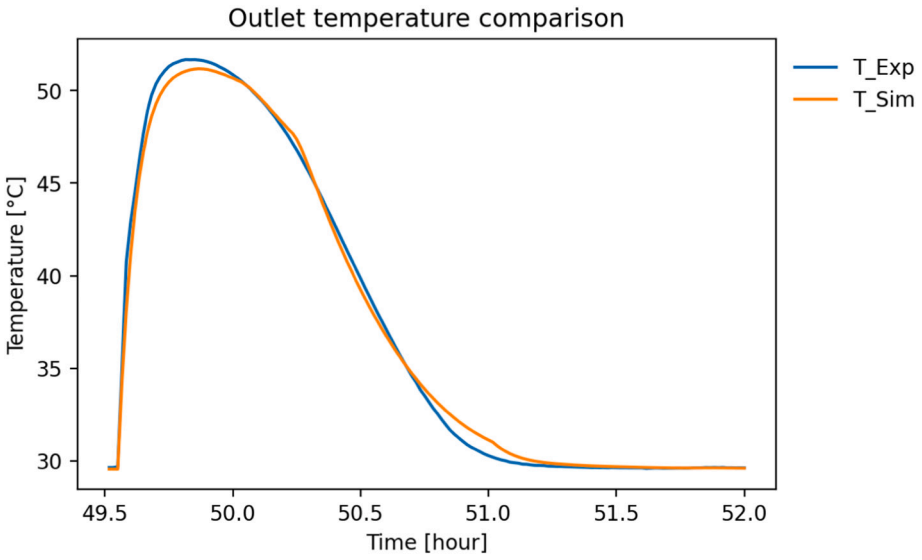

Fig. 17. Experimental and simulated outlet temperature comparison in the PCM solidification period.

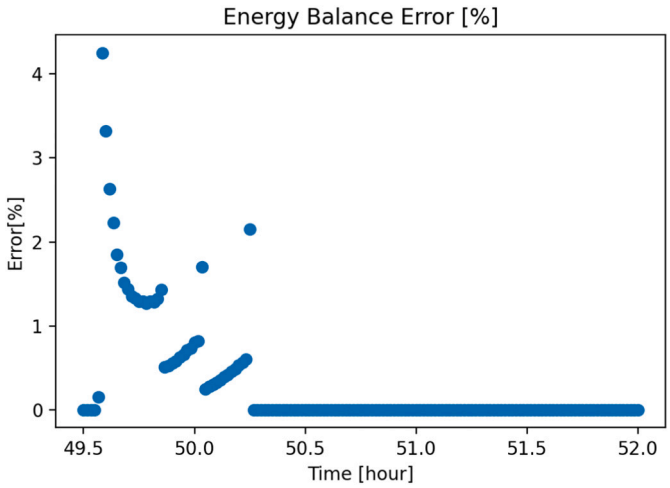

Fig. 18. Energy balance error in the PCM solidification period.

the inlet and the storage. The whole energy storage was kept at 90 °C at the beginning of discharging while the inlet flow temperature dropped immediately from 90 °C to around 30 °C. In this case, it is recommended to increase the tank layers to increase the simulation accuracy, for example, 10 layers. The temperature comparison for the 10 layers model is also shown in green in Fig. 14. It can be seen that the accuracy of the simulated outlet temperature increased a lot for the 10 layers model. The maximum temperature deviation is 4.6 K with the relative error 10.4 %. For the charging and the latent heat discharging periods, the 3 layers model is accurate enough because the inlet flow temperature did not have a large difference with the energy storage temperature and the accumulated numerical error is less in a rough mesh system.

Table 2
Heat content comparison in the three test periods.

	Charged heat (kWh)	Discharged sensible heat (kWh)	Discharged latent heat (kWh)
Experiment	21.7	14.0	7.6
Simulation	21.5	13.9	7.6

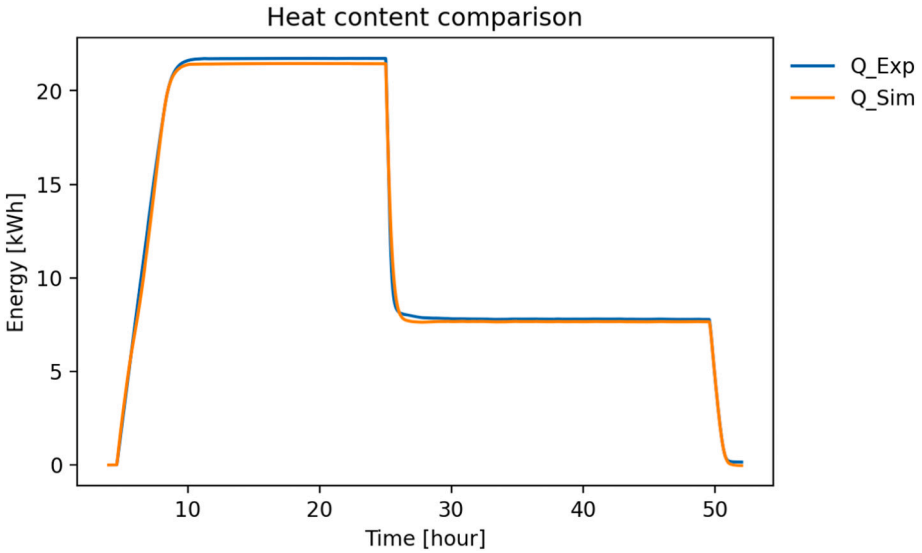

Fig. 19. Experimental and simulated heat content comparison in the full test course.

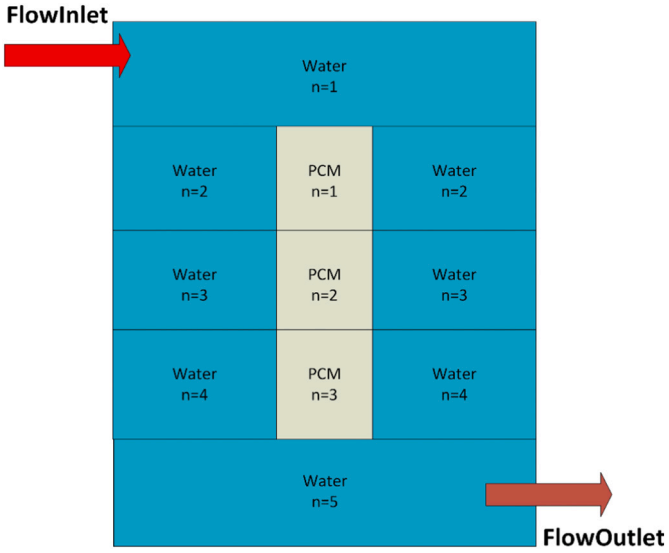

Fig. 20. An example of different layers model of PCM water energy storage.

Figs. 12, 15, and 18 give the total energy balance error in the three simulation periods. It can be seen from the figures that all the energy balance errors are below 5 %, which indicates reasonable simulation processes and good calculation results.

The heat content comparison in the full test period is shown in Fig. 19. The accumulative results of the charging, the sensible heat discharging, and the latent heat discharging period are summed in Table 2, which shows good agreement between the simulation and the experiment. The relative error is within 1 %.

5. Discussion

5.1. Application and limitation

The developed model simulates the temperature and energy development of the energy storage that contains both the PCM and water. Water can be replaced by other sensible fluids with known thermal properties. The solid-liquid PCM should follow the energy–temperature relation as linearized in three sections shown in Fig. 2. For the melting/solidification period, it requires providing the onset and offset temperatures. if only one melting temperature is needed for simulation, users can provide the melting temperature as the onset or offset temperature and assign a slightly different temperature, for example, addling 0.1 °C as another offset or onset temperature.

Since the numerical model is developed by coupling two independent models, the calculation of either the water or the PCM model is encapsulated. Therefore, it is not compulsory requiring the same layers for the PCM and water. The numerical model can simulate an energy storage that PCM and water have different layers. Take the model in Fig. 20 as an example. The water in the outer tank has 5 layers. The PCM locates inside with 3 layers. In this case, the first and last layer of the water model needs to have an updated volume and be given a zero overall heat transfer coefficient Γ to cut off the heat transfer effect. Given the proper settings, the calculation in all the layers can be carried out as normal.

The numerical model can also have changeable layers for different time steps. As explained in the section of experimental verification, when the inlet flow temperature has a larger difference with the energy storage temperature, it is favorable to have a fine mesh structure, in other words, more layers. Since the numerical model is calculated step by step, in one time step, the calculation is only dependent on the given parameters and the input from the last time step. Therefore, it allows assigning a different layer number for different time steps. This feature can increase the calculation efficiency by only assigning more layers for a certain period. The proper layers of the numerical model need to be considered by balancing the calculation accuracy, the accumulated numerical errors, and the calculation efficiency. Typically, the higher temperature difference between the inlet flow and the energy storage, the higher layer numbers are required, and consequently, the higher numerical errors will be accumulated.

The two-model iteration system can be easily extended to, for example, a four-model system with the same solving method, in which the inside heat exchanger and the outside tank wall can be modeled as the other two independent models. The calculation efficiency could be lower than the two-model system, but the extra two temperatures can be obtained.

The numerical model is developed by the Python language [36]. All the calculations in this paper were carried out in the Python environment. It is typically not easy to make system simulations in Python since users should also create numerical models for other components. Therefore, a TRNSYS component Type 7000 for the PCM water numerical mode was created, with the same functionality as the Python model in this paper. Then it is easier for users to use the PCM model in the system calculation. The Type 7000 was also validated by the same experiments in Section 4 under TRNSYS environment [37].

The limitation of the developed model is that it only models and calculates the energy equation and does not consider the momentum (flow) equation in the water tank model. Therefore, the model assumes a uniform flow in the water tank and cannot provide the flow distribution in the tank. Another limitation is that the minimum layers for a numerical model is 2 due to the discrete technique used in the governing equations.

Further, the model is developed in one-dimension. This is appropriate for water model since the water's thermal conductivity and fluidity are good. But for PCM, if the PCM node configuration is only significant in one direction, like the long thin tube in the experiment, the 1D model is appropriate. However, if the PCM node configuration is significant in two dimensions, like a cubic shape, then the 1D model may cause a higher error. In that case, a 2D PCM model is preferred.

5.2. The overall heat transfer coefficient Γ between PCM and water

The overall heat transfer coefficient Γ is the key parameter determining the heat transfer rate between the PCM and water. It describes how fast the energy is transferred between the two materials. The parameter is depended on the design of the internal heat exchanger, the operating condition, and the materials. The parameter needs to be provided by users. There are typically two ways of obtaining the parameter. One is the experimental method. The parameter Γ is calculated from the real test. The difficulty of the experimental method is to measure both the water and PCM temperature, which is not easy to carry out in some circumstances. The other method is the theoretical calculation using CFD simulation or the thermal resistance theory. Consider the thermal resistance theory and take the tubular heat exchanger. PCM is inside the tube while water is flowing outside the tube. The Γ (based on the outer tube area can be calculated as Eq. (31). $1/h_iA_i$ and $1/h_oA_o$ are the inner and outer thermal resistance of the tube while $1/2\pi\lambda \cdot \ln(d_0/d_i)$ is the conduction resistance of the tube material. The heat transfer rate h_i and h_o can be determined according to the practical condition using the empirical equations from the heat transfer textbook [38]. A_i, A_o, d_i, d_o are the inner and outer area and diameter of the tube. λ is the thermal conductivity of the tube material. Other heat exchanger designs will have different Γ equations, but the principle is the same.

$$\Gamma A_o = \frac{1}{\frac{1}{h_iA_i} + \frac{1}{2\pi\lambda} ln\frac{d_o}{d_i} + \frac{1}{h_oA_o}} \tag{31}$$

5.3. Error analysis

The simulation model is developed based on the energy equations, simplified with some key assumptions. Therefore, errors between simulation results and measurements are inevitable. However, the errors need to be constrained within a reasonable scope.

Model simplification error comes from the main assumption that each node has the same temperature, which means the heat transfer effect is neglected in the radical direction in the water and PCM material. The enthalpy curve of the PCM is also simplified into three linearized lines, in which the melting/solidification curve will cause errors since the actual melting/solidification behavior could be more complicated.

Numerical calculation error comes from the discrete of the differential equations. Further, the constant thermal properties of PCM are used in different statuses, which will also cause calculation errors.

The developed numerical model sets up the energy balance error checked in each time step, which is a good tool for users to monitor the errors. Actually, the theory in Section 2.6 was found by the energy balance check. Sometimes, even the temperature profiles are quite similar in the two cases, but if one of the scenarios has a higher energy balance error, that indicates there could be unreasonable settings or calculation errors. Reasonable energy storage configuration, reasonable thermal properties of the PCM, and realistic heat transfer coefficients are the key factors in obtaining reasonable results with small energy balance errors.

The overall heat transfer coefficient Γ between PCM and water is actually always changing during charging and discharging periods. However, if users cannot provide real-time input, the constant value or linearized input also works. In this situation, it is important to have the experimental validation before the final simulation work.

6. Conclusions

A generic numerical model of PCM water energy storage is developed. The numerical model consists of a water region and a PCM region. The two regions are calculated based on the energy conservation equations and solved by the implicit method, which secures stable results. The PCM energy equation is modeled based on the linear enthalpy relations. An iteration method is applied for the two regions for coupling calculation. The extended functionality of the energy storage model is further developed, which includes the separate heat loss coefficients, auxiliary heaters, flexible inlet and outlet, the mixing effect in the water tank, and three PCM supercooling-activation modes.

The numerical model is validated by experiments. A full test sequence for a PCM water energy storage was carried out, including the charging, the sensible heat discharging, and the latent heat discharging period. The energy storage was simulated using the measurements as input. The PCM and water layer temperatures are calculated. The simulated and measured outlet temperature and heat content are compared. The energy balance error is checked at each time step. It shows that the maximum deviation between the measured and simulated outlet temperatures are 2.9 K, 4.6 K, and 2.6 K separately during the charging, the sensible heat discharging, and the latent heat discharging period with the relative error of 5 %, 10.4 % and 6.4 %. The energy balance error is kept within 5 % during all the periods. The measured and simulated heat content in the three periods is quite close, and the relative error is within 1 %. A TRNSYS model is also developed for the numerical model aiming to be used in system simulation.

It can be concluded from the analysis above that

- The developed numerical model is valid for simulating the thermal performance of PCM water energy storage with good accuracy.
- The numerical model can simulate PCM water energy storage with flexible configurations.
- The numerical model is featured with the implicit solving method, accurate calculation for phase change status, encapsulated two-model system, extended functionality, and three PCM supercooling-activation modes.
- Thanks to the encapsulated calculation method, the model can simulate unequal layers of PCM and water and changeable layers during different time steps.

CRediT authorship contribution statement

Weiqiang Kong: Conceptualization, Formal analysis, Methodology, Software, Validation, Visualization, Writing – original draft, Project administration. **Gang Wang:** Investigation, Data curation, Validation. **Gerald Englmair:** Conceptualization, Formal analysis. **Elsabet Nomonde Noma Nielsen:** Conceptualization, Formal analysis. **Janne Dragsted:** Investigation, Project administration. **Simon Furbo:** Project administration, Writing – review & editing. **Jianhua Fan:** Conceptualization, Formal analysis, Methodology, Writing – review & editing.

Declaration of competing interest

The authors declare that they have no known competing financial interests or personal relationships that could have appeared to influence the work reported in this paper.

Data availability

Data will be made available on request.

Acknowledgments

This study was funded by the Danish Energy Agency's Energy Technology Development and Demonstration Program (EUDP) under grant number 64020-2124 and the Bjarne Saxhofs Fond project: *Web based design and simulation platform for solar energy applications*.

References

[1] H. Mehling, L.F. Cabeza, Heat And Cold Storage With PCM: An Up to Date Introduction Into Basics And Applications, Springer, Berlin Heidelberg, 2008 https://books.google.dk/books?id=N8LGwUNYWX8C.
[2] D.N. Nkwetta, P.E. Vouillamoz, F. Haghighat, M. El-Mankibi, A. Moreau, A. Daoud, Impact of phase change materials types and positioning on hot water tank thermal performance: using measured water demand profile, Appl. Therm. Eng. 67 (2014) 460–468, https://doi.org/10.1016/j.applthermaleng.2014.03.051.
[3] A. Sharma, R. Pitchumani, R. Chauhan, Solar air heating systems with latent heat storage - a review of state-of-the-art, J. Energy Storage 48 (2022), 104013, https://doi.org/10.1016/j.est.2022.104013.
[4] O.G. Pop, M.C. Balan, A numerical analysis on the performance of DHW storage tanks with immersed PCM cylinders, Appl. Therm. Eng. 197 (2021), 117386, https://doi.org/10.1016/j.applthermaleng.2021.117386.
[5] R.P. Singh, J.Y. Sze, S.C. Kaushik, D. Rakshit, A. Romagnoli, Thermal performance enhancement of eutectic PCM laden with functionalised graphene nanoplatelets for an efficient solar absorption cooling storage system, J. Energy Storage 33 (2021), 102092, https://doi.org/10.1016/j.est.2020.102092.
[6] J. Li, Y. Zhang, P. Ding, E. Long, Experimental and simulated optimization study on dynamic heat discharge performance of multi-units water tank with PCM, Indoor Built Environ. 30 (2021) 1531–1545, https://doi.org/10.1177/1420326X20961141.
[7] J.F. Belmonte, M. Díaz-Heras, J.A. Almendros-Ibáñez, L.F. Cabeza, Simulated performance of a solar-assisted heat pump system including a phase-change storage tank for residential heating applications: a case study in Madrid, Spain, J. Energy Storage 47 (2022), 103615, https://doi.org/10.1016/j.est.2021.103615.
[8] A. Lecuona, J.I. Nogueira, R. Ventas, M. del C. Rodríguez-Hidalgo, M. Legrand, Solar cooker of the portable parabolic type incorporating heat storage based on PCM, Appl. Energy 111 (2013) 1136–1146, https://doi.org/10.1016/j.apenergy.2013.01.083.
[9] B.C. Anilkumar, R. Maniyeri, S. Anish, Optimum selection of phase change material for solar box cooker integrated with thermal energy storage unit using multi-criteria decision-making technique, J. Energy Storage 40 (2021), 102807, https://doi.org/10.1016/j.est.2021.102807.
[10] M. Yasin, E. Scheidemantel, F. Klinker, H. Weinläder, S. Weismann, Generation of a simulation model for chilled PCM ceilings in TRNSYS and validation with real scale

building data, J. Build. Eng. 22 (2019) 372–382, https://doi.org/10.1016/j.jobe.2019.01.004.
[11] X. Sun, Y. Zhang, K. Xie, M.A. Medina, A parametric study on the thermal response of a building wall with a phase change material (PCM) layer for passive space cooling, J. Energy Storage 47 (2022), 103548, https://doi.org/10.1016/j.est.2021.103548.
[12] M. Dardir, K. Panchabikesan, F. Haghighat, M. El Mankibi, Y. Yuan, Opportunities and challenges of PCM-to-air heat exchangers (PAHXs) for building free cooling applications—a comprehensive review, J. Energy Storage 22 (2019) 157–175, https://doi.org/10.1016/j.est.2019.02.011.
[13] G. Liu, Q. Li, J. Wu, R. Xie, Y. Zou, A. Marson, A. Scipioni, A. Manzardo, Improving system performance of the refrigeration unit using phase change material (PCM) for transport refrigerated vehicles: an experimental investigation in South China, J. Energy Storage 51 (2022), https://doi.org/10.1016/j.est.2022.104435.
[14] S. Morales-Ruiz, J. Rigola, C. Oliet, A. Oliva, Analysis and design of a drain water heat recovery storage unit based on PCM plates, Appl. Energy 179 (2016) 1006–1019, https://doi.org/10.1016/j.apenergy.2016.07.067.
[15] C. Zauner, F. Hengstberger, M. Etzel, D. Lager, R. Hofmann, H. Walter, Experimental characterization and simulation of a fin-tube latent heat storage using high density polyethylene as PCM, Appl. Energy 179 (2016) 237–246, https://doi.org/10.1016/j.apenergy.2016.06.138.
[16] V. Ljungdahl, K. Taha, J. Dallaire, E. Kieseritzky, F. Pawelz, M. Jradi, C. Veje, Phase change material based ventilation module - numerical study and experimental validation of serial design, Energy 234 (2021), 121209, https://doi.org/10.1016/j.energy.2021.121209.
[17] K. Filonenko, V.B. Ljungdahl, T. Yang, C. Veje, Modelica implementation of phase change material ventilation unit, in: 6th IEEE Int.Energy Conf. ENERGYCon2020, 2020, pp. 464–467, https://doi.org/10.1109/ENERGYCon48941.2020.9236495.
[18] The Modelica Association (n.d.), https://modelica.org/.
[19] Y.B. Tao, Y.L. He, Y.K. Liu, W.Q. Tao, Performance optimization of two-stage latent heat storage unit based on entransy theory, Int. J. Heat Mass Transf. 77 (2014) 695–703, https://doi.org/10.1016/j.ijheatmasstransfer.2014.05.049.
[20] Y.B. Tao, Y.L. He, Effects of natural convection on latent heat storage performance of salt in a horizontal concentric tube, Appl. Energy 143 (2015) 38–46, https://doi.org/10.1016/j.apenergy.2015.01.008.
[21] IEA SHC Task 32, Advanced storage concepts for solar and low energy buildings (n.d.), https://task32.iea-shc.org/.
[22] W. Streicher, J. Bony, S. Citherlet, A. Heinz, P. Pusching, H. Schramzhofer, J. M. Schultz, Simulation models of PCM storage units. http://ww.iea-shc.org/publications/downloads/task32-c5.pdf, 2008.
[23] U. of W.–M.S.E. Laboratory, TRNSYS, A Transient Simulation Program, The Laboratory, Madison, Wis., 1975 https://search.library.wisc.edu/catalog/999800551102121.
[24] J. Bony, S. Citherlet, Extension of a Trnsys model for latent heat storage with phase change materials used in solar water tank (n.d.), in: Ecostock 2006, 2006.
[25] J. Bony, S. Citherlet, Numerical model and experimental validation of heat storage with phase change materials, Energy Build. 39 (2007) 1065–1072, https://doi.org/10.1016/j.enbuild.2006.10.017.
[26] M. Abbasi Kamazani, C. Aghanajafi, Numerical simulation of geothermal-PVT hybrid system with PCM storage tank, Int. J. Energy Res. 46 (2022) 397–414, https://doi.org/10.1002/er.7279.
[27] J.F. Belmonte, P. Eguía, A.E. Molina, J.A. Almendros-Ibáñez, R. Salgado, A simplified method for modeling the thermal performance of storage tanks containing PCMs, Appl. Therm. Eng. 95 (2016) 394–410, https://doi.org/10.1016/j.applthermaleng.2015.10.111.
[28] W. Tao, Numerical Heat Transfer, 2nd ed., Xi'an Jiaotong University Publishing Company, 2001 (In Chinese).
[29] S.V. Patankar, Numerical heat transfer and fluid flow, Hemisphere Publishing Corporation, 1980. https://books.google.dk/books?id=N2MVAQAAIAAJ.
[30] M. Carmona, A. Rincón, L. Gulfo, Energy and exergy model with parametric study of a hot water storage tank with PCM for domestic applications and experimental validation for multiple operational scenarios, Energy Convers. Manag. 222 (2020), 113189, https://doi.org/10.1016/j.enconman.2020.113189.
[31] TESSLibs 17 - Storage Tank Library Mathematical Reference. Type 534: Vertical Cylindrical Storage Tank with Immersed Heat Exchanger, 2014.
[32] M. Dannemand, J.B. Johansen, W. Kong, S. Furbo, Experimental investigations on cylindrical latent heat storage units with sodium acetate trihydrate composites utilizing supercooling, Appl. Energy 177 (2016) 591–601, https://doi.org/10.1016/j.apenergy.2016.02.038.
[33] G. Wang, M. Dannemand, C. Xu, G. Englmair, S. Furbo, J. Fan, Thermal characteristics of a long-term heat storage unit with sodium acetate trihydrate, Appl. Therm. Eng. 187 (2021), 116563, https://doi.org/10.1016/j.applthermaleng.2021.116563.
[34] G. Wang, C. Xu, G. Englmair, W. Kong, J. Fan, S. Furbo, G. Wei, Experimental and numerical study of a latent heat storage using sodium acetate trihydrate for short and long term applications, J. Energy Storage 47 (2022), 103588, https://doi.org/10.1016/j.est.2021.103588.
[35] HM Heizkörper GmbH. https://hm-heizkoerper.de, 2022.
[36] Python official website. https://www.python.org/, 2022.
[37] G. Wang, Flexible Phase Change Thermal Storage Study Based on Stable Supercooling of Sodium Acetate Trihydrate, Ph.D thesis, Technical University of Denmark, 2022.
[38] S. Yang, W. Tao, Heat Transfer, 3rd ed., Higher Education Press, Beijing, 1998.